Multidiszciplináris Tudományok, 14. kötet, 3. szám (2024) pp. 114-130. **https://doi.org/10.35925/j.multi.2024.3.10**

MICROSTRUCTURAL CHARACTERISTICS OF HYDROGEN-EXPOSED P355NH STEEL AND WELDED JOINTS

Nóra Nagy
assistant lecturer, University of Miskolc, Institute of Material Science and Technology
Department of Structural Integrity
3515 Miskolc, Miskolc-Egyetemváros, e-mail: nora.nagy@uni-miskolc.hu

Abstract
It is known that microstructure of materials, such as material structure, grain size, orientation, crystallographic texture and dislocation density, change the mechanism and intensity of hydrogen diffusion, contribute to an increase or decrease in solubility, which significantly changes the mechanical properties of steels and leads to brittleness. In the present study, the microstructure of welded joints of steel P355NH, a typical material grade in domestic transmission lines, and GMAW and hybrid GTAW /GMAW welded joints were investigated and exposed to high pressure pure hydrogen with exposure times of 41 and 92 days. The investigations were carried out to find out the characteristic microstructural details of the base material and welded joints, and the mechanical property changes that can be observed, which can be used to infer the hydrogen susceptibility of both the base material and the welded joints.

Keywords: *high pressure hydrogen, transmission pipeline steel, microstructure*

1. Introduction

Hydrogen atoms, due to their small size, are able to penetrate the microstructure of steel and interact with different parts of the microstructure, causing structural defects that lead to a reduction in the plastic deformation of the steel and the formation of cracks. The material structure of pipeline steels is always inhomogeneous, and there are also lattice defects, so the diffusion of hydrogen in the steel is not based on a single factor. Some microstructural features may be so-called hydrogen traps, which can promote the accumulation of hydrogen in the material structure. From a thermodynamic point of view, traps represent a lower chemical potential for hydrogen and require a higher activation energy to pass through them. Their binding energy to hydrogen, the size and morphology of the traps influence the reversible or irreversible nature of the trap (Oriani, 1970).

Hydrogen diffusion into the microstructure of steels occurs in three steps.

1. Physical adsorption, which takes place on the surface. In this case, weak van der Waals forces act on the interfaces, resulting in the absorption of hydrogen atoms.
2. Chemical absorption is a chemical reaction between hydrogen atoms and the surface of steel.
3. Finally, in the last step, hydrogen diffuses into the crystal structure of the steel (Anijdan, 2021).

2. Microstructural aspects of hydrogen embrittlement

Diffusion of hydrogen in crystalline materials can occur by several mechanisms, based on the crystalline location of atomic motion, there is so-called substitutional (vacancy) and interstitial diffusion. The

probability of interstitial diffusion is much higher in the crystal lattice because the probability of interstitial vacancies is higher and the degree of lattice distortion caused will be higher due to the size difference of the atoms (Brass et al., 2000). Hydrogen interstitially positioned in face-centered cubic (fcc) lattices tends to prefer octahedral sites, whereas in body-centered cubic (bcc) crystals it is positioned in tetrahedral sites. According to Wipf (Wipf, 2001), the distance between octahedral sites in surface-centered crystal structures of metals is almost twice the distance between tetrahedral interstitial sites in space-centered lattices. As a result, hydrogen diffusion is generally smaller in metals with fcc lattices than in metals with bcc lattices.

Interstitial hydrogen also modifies the local electron structure of the metal atom, because it can transfer some or all of its electric charge to neighbouring atoms. This can reduce the cohesion between atoms and lead to the formation of cracks (Brass et al., 2000). This is one of the basic concepts among the many theories on which the phenomenon of hydrogen-induced embrittlement (HE) has been developed. The hydride-induced embrittlement (HEDE) model (Westlake, 1969) is related to hydrogen supersaturation, but is mainly concerned with austenitic steels (Chene, 1982) because of the low solubility of hydrogen in the lattice in ferritic steels (Brass et al., 2000). The hydrogen-vacancy approach (Fukai, 2001) is based on the ability of hydrogen to create new vacancies (Superabundant Vacancy) and to stabilize them. It can be assumed that the formation of SAV vacancies is probably caused by the interaction of hydrogen with pre-existing vacancies, mainly at grain boundaries. An increase in the number of vacancy sites leads to the formation of microcracks or microcavities at these sites (Takai et al., 2008). Experiments by Takai (Takai et al., 2008) have demonstrated that vacancy alone is responsible for the reduction in ductile deformation in the presence of hydrogen.

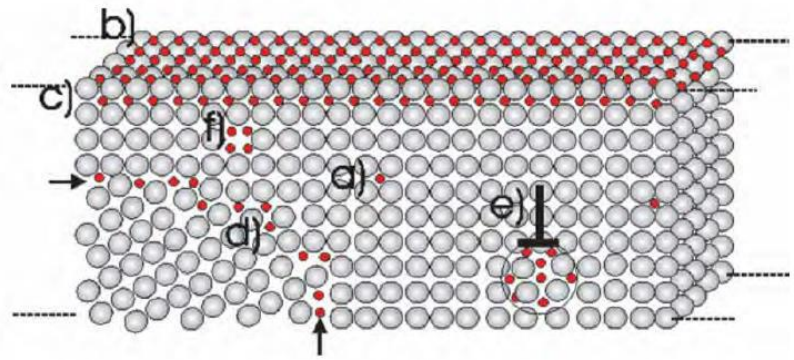

Figure 1. *Microstructural parts where hydrogen can accumulate: (a) at the lattice: surface (b), sub-surface (c); grain boundary (d), dislocation (e) vacancy (f) (Pundt, 2006).*

In the theory of hydrogen-induced plasticity, the hydrogen-dislocation interaction is one of the main mechanisms that influence it. Within this theory, two main mechanisms are mentioned: adsorption-induced dislocation emission (AIDE) (Lynch, 1988) and hydrogen-induced local plasticity (HELP) (Beachem, 1972). The AIDE mechanism states that adsorbed hydrogen reduces the energy of dislocation formation, resulting in a reduction of the stress required to emit dislocations. According to the HELP mechanism, dissolved hydrogen facilitates the movement of dislocations, leading to local plastic deformation and a reduction in the critical stress required for crack formation.

Polycrystalline materials have more grain boundaries and thus more lattice defects, which favours atomic diffusion, but the microstructure also plays an important role in hydrogen trapping. If we look at the microstructure of the material, it can be said that perlite is more prone to hydrogen-induced cracking

than a material structure composed of pure ferritic phases, due to the higher hardness and brittleness of perlite. Hydrogen atoms agglomerate in the ferrite grain boundaries between the plates of the perlite, but the cementite plates in the perlite also hinder the passage of hydrogen but are not considered irreversible traps due to their low energy (Anijdan, 2021). Park (Park et al., 2008) investigated hydrogen traps in different structures in API X65 steels and concluded that certain microstructures such as perlite, needle ferrite, bainite and martensite/austenite ratio affect both hydrogen adsorption and hydrogen diffusion in the microstructure. It is found that the binding efficiency increases in the order of perlite, bainite, ferrite. When the permeability of the different phases is considered, bainite has lower permeability than perlite. Studies have shown that the martensite phase exhibited the highest resistance to hydrogen diffusion, while the hardened martensite showed the lowest (Parvathavarthini, 1999). In the case of perlite, the interface between the ferrite and cementite phases is considered to be dominant for hydrogen bonding, while the cementite in the fine sheet bainite hinders hydrogen diffusion (Tau, 1996; Luu, 1996). Chan (Chan et al., 1991) studied residual austenite in a martensitic structure and concluded that no significant hydrogen is dissolved into the austenite remaining between the martensitic phase, but that the interface between residual austenite and martensite is a possible hydrogen trap. Therefore, the residual austenite in steel plays a key role in the diffusion of hydrogen. Sakamoto (Sakamoto, 1976) investigated the effect of quenching and tempering and found that quenched martensite has minimum diffusivity and maximum solubility compared to quenched and tempered martensite. The lowest diffusion values were measured in martensite in API X70 steel (Olden et al., 2012). It has been observed that the martensite phase has the lowest hydrogen solubility, but the solubility increases with increasing annealing temperature and reaches a maximum value when annealing at 300 °C (Newman, 2010). Fallahmohammadi (Fallahmohammadi et al., 2014) investigated hydrogen in API X65 and low alloy F22 steels in quenched, tempered and annealed condition, where he showed that the irreversible trapped hydrogen was highest in the annealed samples.

Dislocations are considered reversible hydrogen traps due to their low binding energy (Choo, 1983). The interaction between hydrogen and dislocations can be explained by the Cottrell atmosphere around the dislocations (Cotterill, 1961). At the base of dislocations, hydrogen accumulates and hinders the movement of dislocations, causing local deformation hardening, which reduces plastic deformation and leads to an increase in strength properties (Stalheim, 2010). Cabrini (Cabrini et al., 2020) investigated the consequences of an increase in dislocation density on hydrogen diffusion in low alloy steels and found that as dislocation density increases, apparent diffusion decreases. During cyclic plastic deformation, immobilized dislocations accumulated on grain boundaries increased the number of hydrogen traps and thus hydrogen diffusion became limited (Jiang et al., 2021).

Grain boundaries are reversible hydrogen traps through which hydrogen diffuses more rapidly, so in general fine-grained materials have a higher resistance to fracture. Studies have shown that the diffusion rate of hydrogen increases in fine-grained microstructures, but the opposite effect has also been observed for triple junctions, which can act as potential hydrogen traps and reduce the diffusion of hydrogen (Ichimura, 1991).

These structural factors play a key role in the diffusion or binding of hydrogen. It can also be seen that the optimum microstructural characteristics for hydrogen resistance do not always meet the requirements for production and operation.

3. Investigated P355NH steel and welded joints

In our research, we tested steel and welded joints of P355NH material grade exposed to pure hydrogen at 128 bar pressure (twice the MAOP) with exposure times of 41 and 92 days. Microscopic images were taken with a Zeiss Axio Observer Dm1 inverted optical microscope. The material microstructure is ferrite-pearlite, with a ferrite-pearlite structure ratio of approximately 80%-20%. Full-scale tests were carried out on the pipeline sections prior to the hydrogen tests (Lukács, 2024). The ferrite grains in rows indicates plastic deformation.

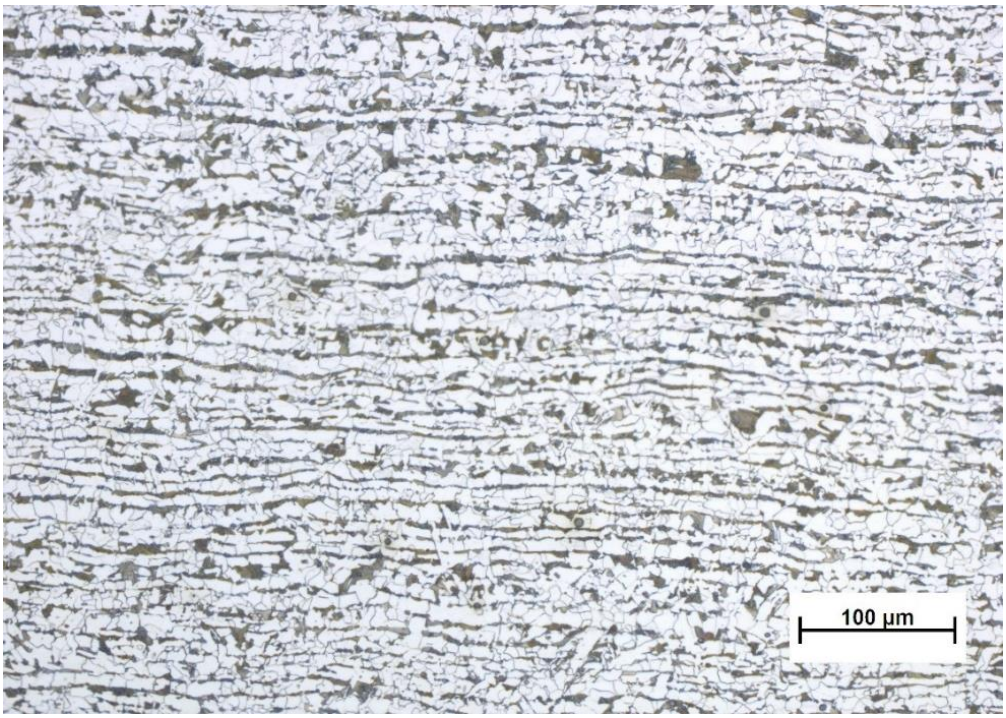

Figure 2. *Ferrite-pearlite material structure of the pipeline section base material, N=200x, etched: 2% HNO_3*

The welded joints that remained intact during the full-scale tests were made by GMAW, and the welds for the hydrogen testing of pipe sections were made by GTAW/GMAW (Figure 3). The tested girth welds were made under industrial conditions using manual gas metal arc welding, while the new, girth welds applying TIG welding with solid filler rode material (root) and manual gas metal arc welding (further layers). The main parameters of the welding processes are contained in Tables 1 and 2. The heat-affected zone of the welded steels can be divided into several zones. During welding, the change in hardness and toughness is critical mainly in the intercritical (partially transformed) and grain growth zones, but in the case of hydrogen exposure, it can also occur in the fine grain zone, with even larger increases in hardness and decreases in toughness.

Table 1. *Main characteristics of GMAW weld processes*

Layer	**1st (root)**	**2nd**	**3rd**
Position	PH	PJ	PJ
Filler metal	Böhler FOX CEL	Böhler FOX CEL Mo	Böhler FOX CEL Mo
Diameter, mm	3.2	3.2	3.2
Current, A	DC/EN 45-55	DC/EP 55-70	DC/EP 50-65
Voltage, V	21.8-22.2	22.2-22.8	22.0-22.6
Welding speed, cm/min	7-12	15-20	10-15

Table 2. *Main characteristics of the GTAW/GMAW weld processes*

Layer	**1st (root)**	**2nd**	**3rd**
Position	PA	PA	PA
Filler metal	OK Tigrod 12.64	OK 48.00	OK 48.00
Diameter, mm	2.0	2.5	3.2
Current, A	DC/EN 80-90	DC/EP 80-85	DC/EP 100-105
Voltage, V	21.8-22.2	22.2-22.8	22.0-22.6
Welding speed, cm/min	7-12	15-20	10-15

Figures 3 and 4 show the microscopic images of the heat-affected zones of the joints.

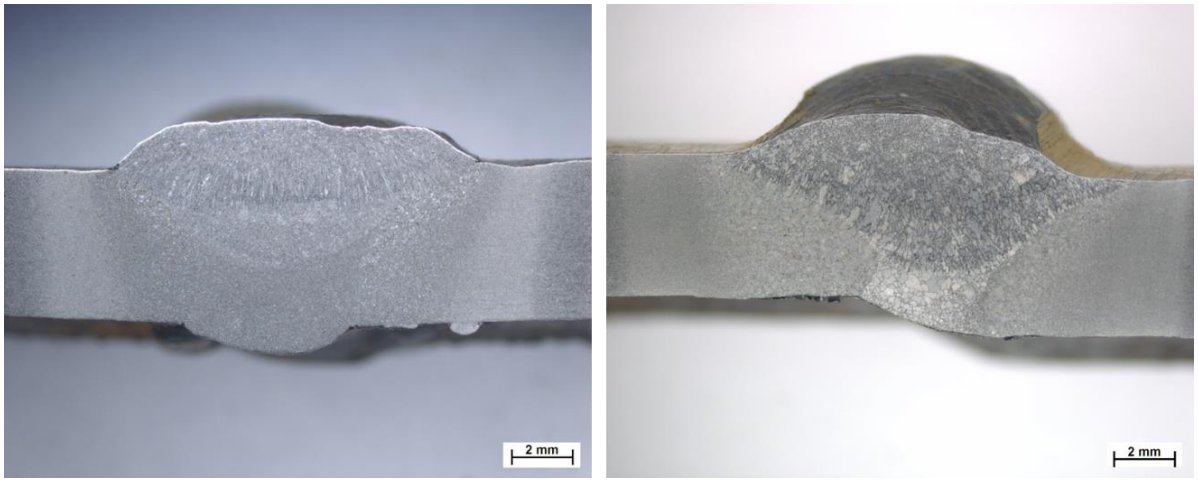

a) GMAW *b) hybrid*

Figure 3. *Macro images of the welded joints tested, N=6,5x*

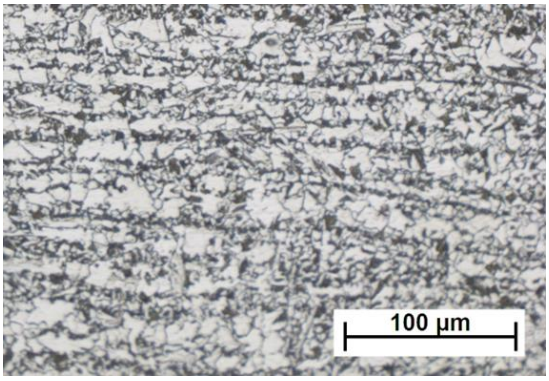

a) Intercritical zone

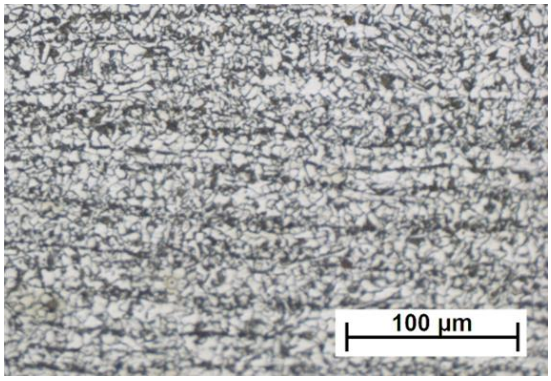

b) Recrystallisation zone

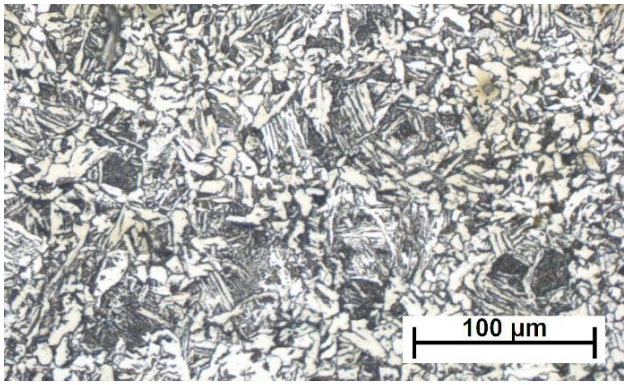

c) Grain-growth zone

Figure 4. *Typical microstructures of welded joints in the heat-affected zone, =200x, etched: 2% HNO_3*

The images clearly show that in the intercritical zone, after dissolution and decomposition of the perlite, a much smaller grain size perlite structure is formed, but typically with a higher carbon content, because the carbon dissolution capacity of austenite is high at temperatures between A1-A3. In this zone, most of the ferrite is identical to the original, initial microstructure. In the fine-grained zone, a typical recrystallisation process takes place, where a fine-grained ferrite-pearlite microstructure is formed from austenite. In the grain growth zone, non-equilibrium formations (bainite, martensite) appear in the structure as it cools. Figure 5 shows the microstructure of the weld roots made using two different welding techniques, where the multiple heat input also results in the predominance of non-equilibrium formations (bainite, tempered martensite), but in apparently different proportions. On the new welded joints after full-scale tests, where the roots were prepared by GTAW technology, no tests were performed in the pre-exposure state to hydrogen.

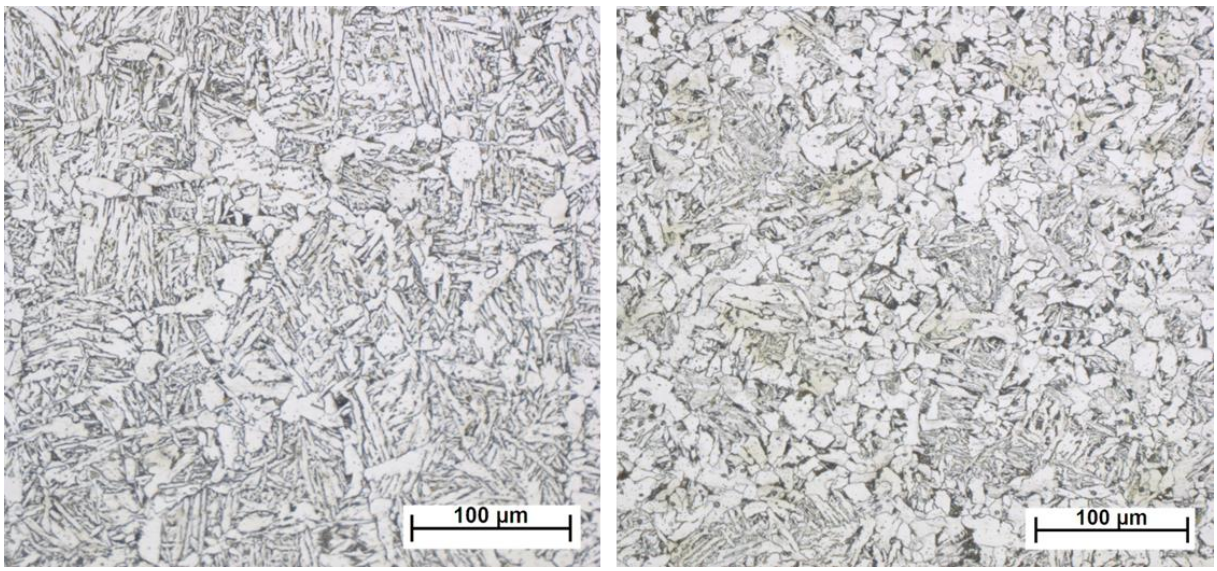

a) GMAW root *b) GTAW root*

Figure 5. *Microstructure of the weld roots, N=200x, etched: 2% HNO_3*

4. Measurements of Hardness

4.1. Microhardness measurement

For the hardness average values, samples of both the base material and the welded joints were taken from both the non-hydrogen and hydrogenated pipeline sections near the hydrogen exposed surfaces. Microhardness measurements were performed using a Mitutoyo MVK-H1 hardness tester to determine the average of hardness of the ferrite and pearlite elements of the base material at a load of 10 grams. The hardness of pearlite increased more after 41 days: ΔHV5=50 HV than that of ferrite, where the difference was: ΔHV5=25 HV (Figure 6).

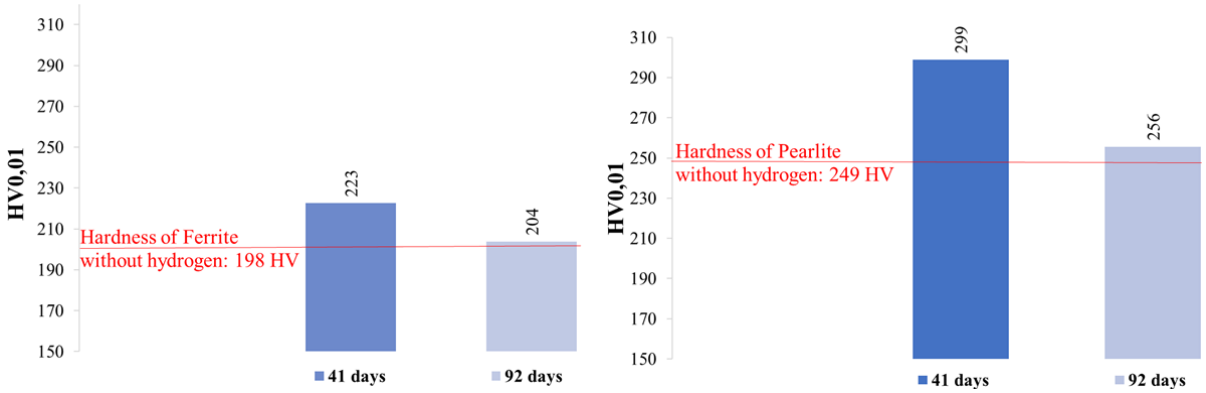

Figure 6. *Results of microhardness measurement in the microstructure of the base material*

4.2. Macrohardness measurement

Macrohardness was measured using a Wilson-Hardness Reicherter UH-250. HV5 hardness values were determined, in accordance with microscopic images, to distinguish the heat-affected zones of the welded joints. In the diagrams, the samples marked with an H indicate the exposure to hydrogen. Of the pipe sections, pipeline section HY4 was exposed to pure hydrogen for 41 days and HY9 for 92 days.
Figure 7 shows that the hardness of the base material increased as a result of hydrogen exposure, but again the increase was greater in the 41-days case.

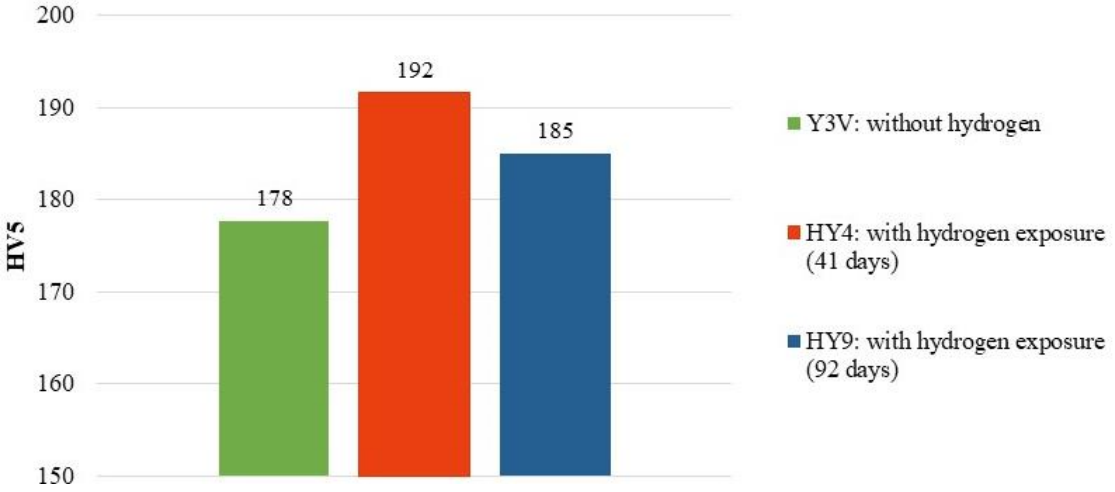

Figure 7. *Hardness of the base material after exposure times of 41 and 92 days*

For the welded joints, V indicates a GMAW root and W indicates a GTAW root.

The intercritical zone of HY4V joints showed the largest increase in the 41-days case (ΔHV5=17 HV). There was no significant difference in hardness values for HY4W and HY9W welded joints (Figure 8). The Figure 9 shows that the intercritical zone of the heat-affected zones in HY4W has a slightly finer grain size of ferrite, suggesting that more ferrite is dissolved in this zone due to the higher temperature than in HY4V.

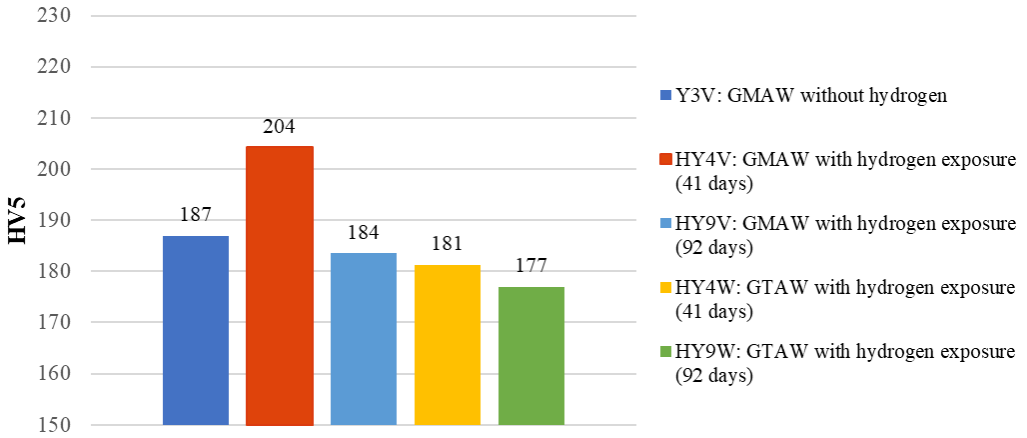

Figure 8. *Results of hardness measurements in the intercritical zone of the heat-affected zone*

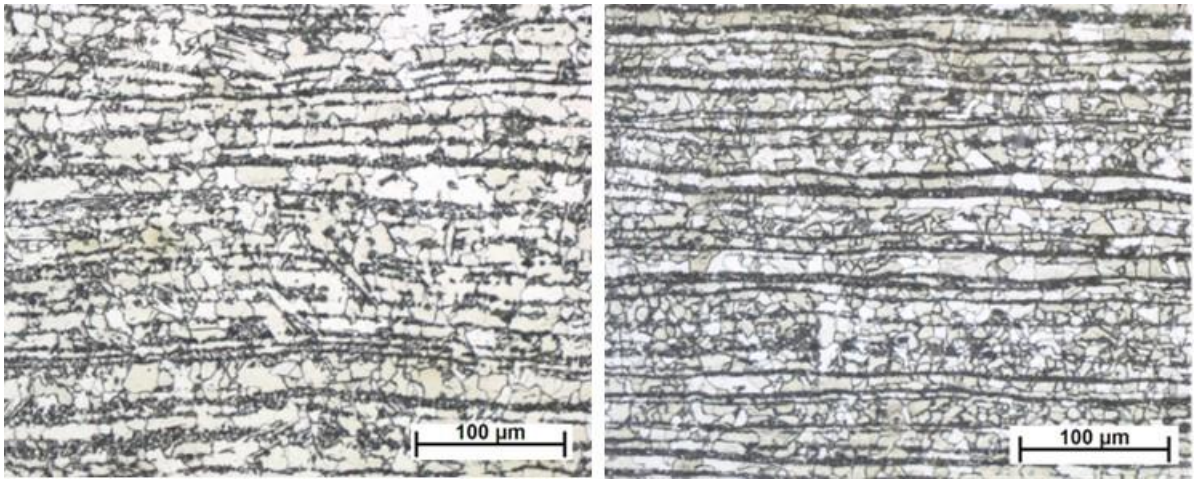

a) HY4V *b) HY4W*

Figure 9. *Intercritical zones of the heat-affected zone of welded joints, N=200x, etched: 2% HNO_3*

For the recrystallization zone (Figure 10), a significant increase in hardness is observed in the joints made by the GMAW process. For 41 days of exposure to hydrogen the change in hardness is ΔHV5=22 HV, after 92 days ΔHV5=15 HV. The hardness of the joints prepared with the GTAW root did not change significantly after 92 days of exposure to hydrogen. A typical record of the recrystallization zone for joints prepared with different processes is shown in Figure 11. In the microscopic images, the root side of the HY4W joint retains the texture and the row ordering and the grain size is visually larger than in the HY4V joint. This suggests that recrystallisation has not fully occurred in the HY4W joint.

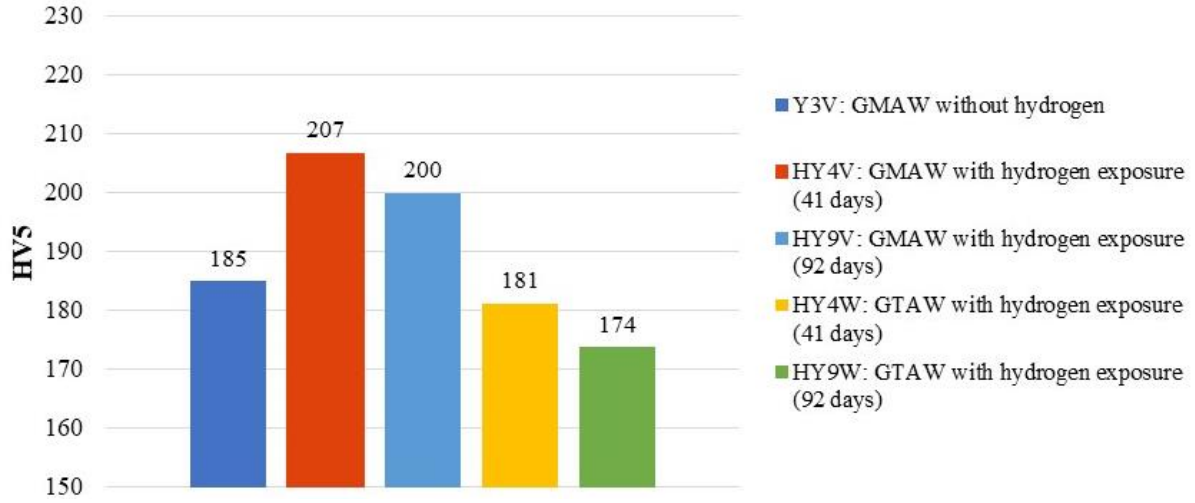

Figure 10. *Results of hardness measurements in the recrystallisation zone of the heat-affected zone*

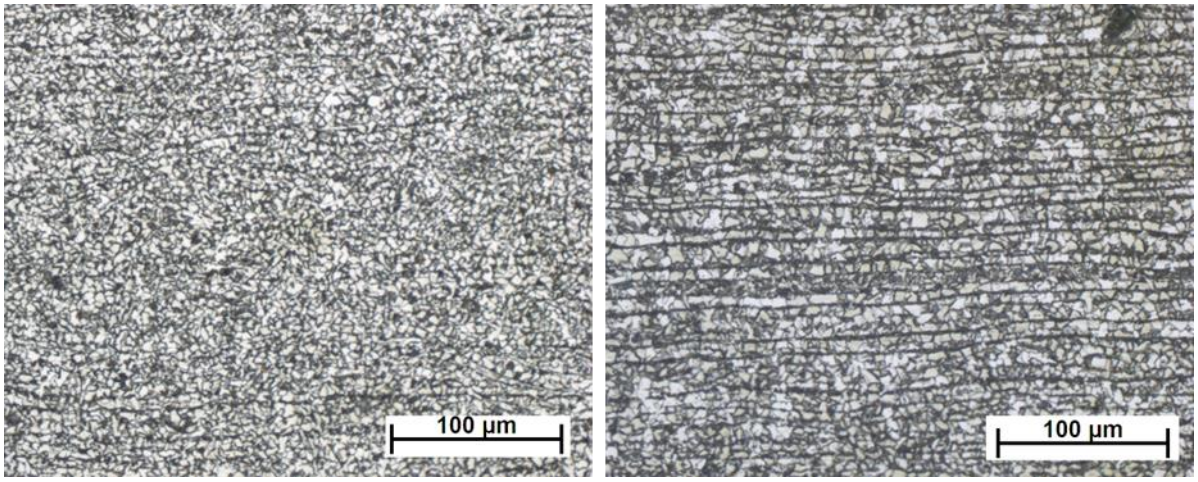

a) HY4V *b) HY4W*

Figure 11. *Recrystallisation zones in the heat-affected zone of welded joints, N=200x, etched: 2% HNO_3*

In the grain growth zones of the joints (Figure 12), both GMAW and GTAW/GMAW joints show a significant increase in hardness. For 41 days of exposure to hydrogen, the hardness change in the HY4V joint is ΔHV5=17 HV. After 92 days, the hardness increase is ΔHV5=27 HV. In the grain growth zone of the HY4W joint, the hardness increase after 92 days of exposure is ΔHV5=14 HV. Looking at the microstructure, it can be observed that the coarse grain size of the HY4W joint is about twice that of the HY4V joints (Figure 13). This can be attributed to the result of the HY4W joints heating to higher temperatures.

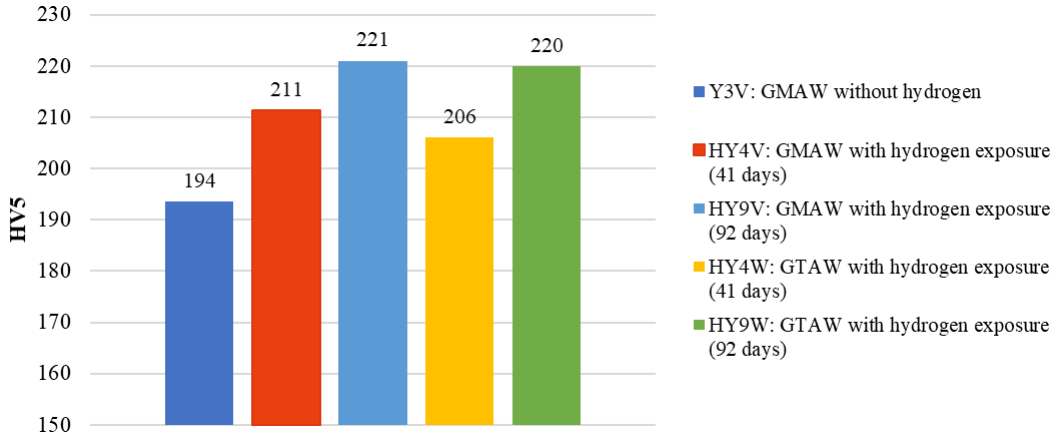

Figure 12. *Results of the hardness measurement in the grain growth zone of the heat-affected zone*

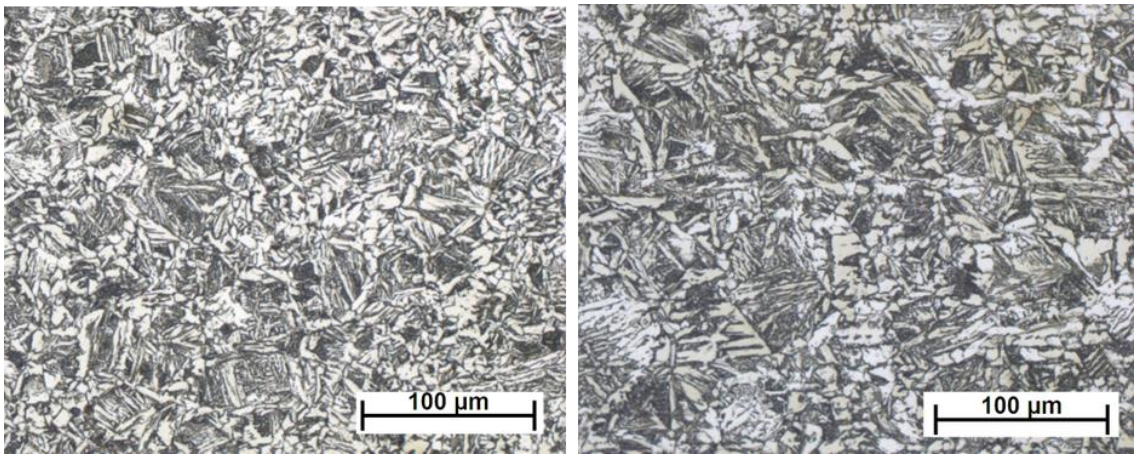

a) HY4V *b) HY4W*

Figure 13. *Grain growth zones in the heat-affected zone of welded joints, N=200x, etched: 2% HNO_3*

Based on the hardness values measured on the weld root, it can be concluded that the GMAW joints showed a smaller increase in hardness. For 41 days of exposure to hydrogen, the change in hardness in HY4V joint ΔHV5=11 HV. In HY9V joint, the increase in hardness after 92 days ΔHV5=15 HV. The hardness of GTAW root did not change significantly after 92 days of exposure to hydrogen.

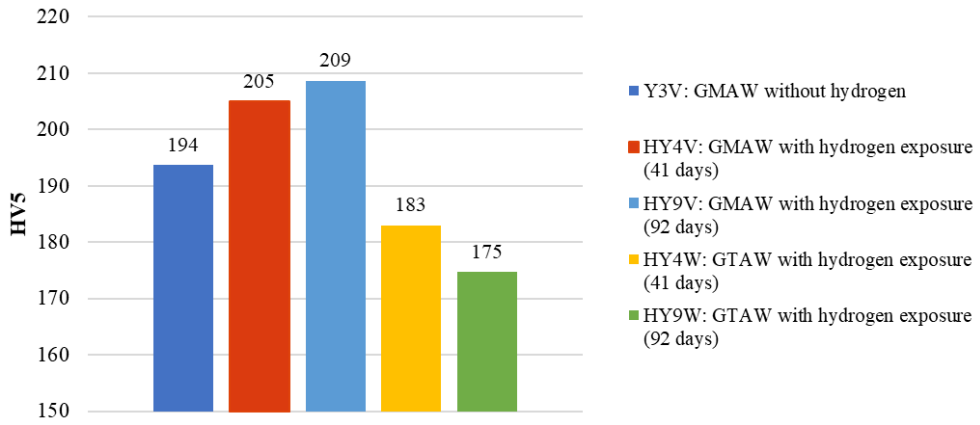

Figure 14. *Results of the hardness measurement in the weld root*

In the microstructure of the weld roots already shown in Figure 4, there are different proportions of bainitic and tempered martensitic parts. It can be clearly seen that while the amount of tempered martensite is obviously higher in the case of GTAW weld root than in the case of GMAW radicals.

4.3. Assessment of hardness measurements

From the microhardness values of the microstructure of the base material, it can be seen that both ferrite and pearlite have increased hardness. The increase in the hardness of perlite can be attributed to the fact

that the body centered cubic ferrite can hold hydrogen, the ferrite-cementite phaseboundaries in the perlite act as hydrogen traps. Exposure to hydrogen for 92 days did not cause significant changes in any microstructure. This may be because the phase interfaces in the pearlite are reversible traps and even a small activation energy is sufficient to trigger further diffusion of hydrogen in the steel.

For welded joints, the hardness values of GMAW joints in the intercritical zone increased slightly. The images show the oriented texture due to the previous plastic deformation. The plastic deformation leads to an increase in dislocation density, which favours hydrogen diffusion by creating new diffusion paths in the microstructure (pipediffusion). In the intercritical zone, a larger fraction of the ferrite in the GTAW bond was dissolved, resulting in smaller ferrite grain size, but the oriented texture is still observed.

In the recrystallisation zone, a significant increase in hardness is observed for GMAW joints. The oriented texture is no longer visible in the images after recrystallisation. The decrease in grain size in this case resulted in a significant increase in hardness. The recrystallisation of the GTAW joint did not take place completely, although the grain size was also reduced, but not to the same extent as in the case of the GMAW joints. The oriented texture is still visible in this case. t is likely that these two effects resulted in the hardness values not increasing in the intercritical and recrystallization zones under the influence of hydrogen in the case of the GTAW joint.

The largest differences in the grain growth zone, for both GMAW and GTAW joints. For the root composition, bainite has lower diffusion and higher solubility compared to tempered martensite, which may be the reason why GTAW root hardness did not increase with hydrogen, while GMAW root hardness did.

5. Tensile test

To determine the strength and deformation indices of the base material, a tensile test was carried out on a universal material tester MTS 810.23. The strain of cylindrical samples of proportional length with nominal diameter d_0 = 4 mm was measured using an extensometer. The force-displacement (F-ΔL) values recorded during the test were recorded. For the tests, 3-3 samples were prepared and the average of the test results is summarized in Table 3.

Table 3. *Results of the tensile test*

Sample nomination		**R_m, [MPa]**	**$R_{p0,2}$, [MPa]**	**A, [%]**	**Z, [%]**
Y3	*without hydrogen*	581	492	16	76
HY4	*hydrogen exposure: 41 days*	619	511	15	74
HY9	*hydrogen exposure: 92 days*	607	494	12	73

To accurately determine the reduction of area, the typical dimensions of the samples were measured using a Zeiss Stemi 2000-C stereo microscope (Figure 15).

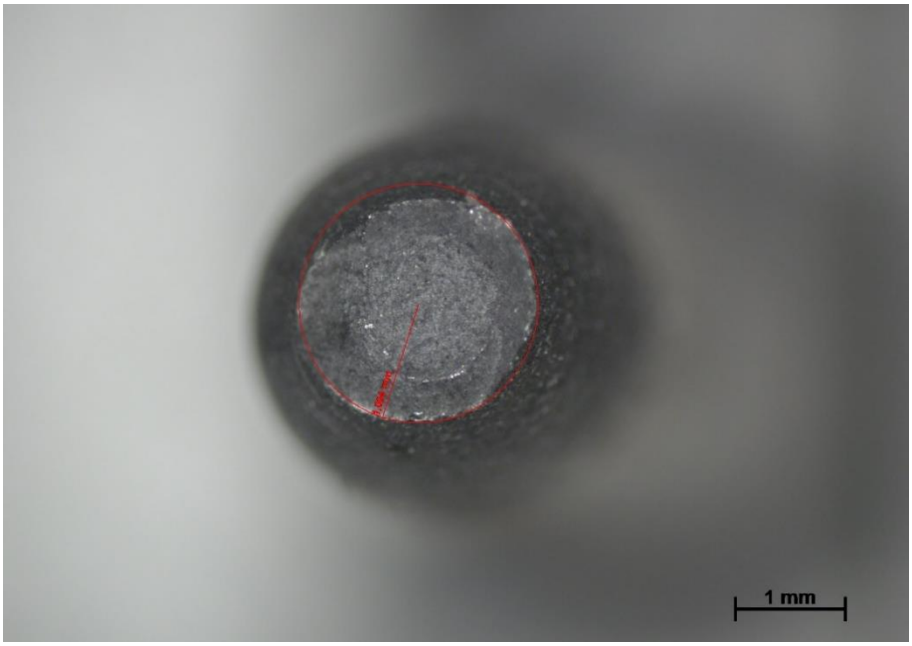

Figure 15. *Measuring the surface area of the sample using an optical microscope, N=16x*

From the results, it can be concluded that the specified strength properties (tensile strength, yield strength) increased due to hydrogen exposure, while the strain properties (elongation, reduction of area) decreased.

The characteristic diagrams recorded during the tensile test are shown in Figure 16.

In Figure 16, the yield phenomena that appear in the hydrogen-exposed samples are related to the movement of the dislocations that produce the plastic deformation. The interstitially dissolved hydrogen accumulated at the base of the dislocations essentially hinders the movement of the dislocations, resulting in an increase in the critical slip stress required for plastic deformation, and therefore further deformation can only be achieved with increasing load. However, the resulting Cottrell atmosphere is not an irreversible trap and a small activation energy of hydrogen is sufficient to diffuse into the dislocation, thereby reducing the critical slip stress for initiating plastic deformation and causing the dislocations to move under the effect of a smaller load.

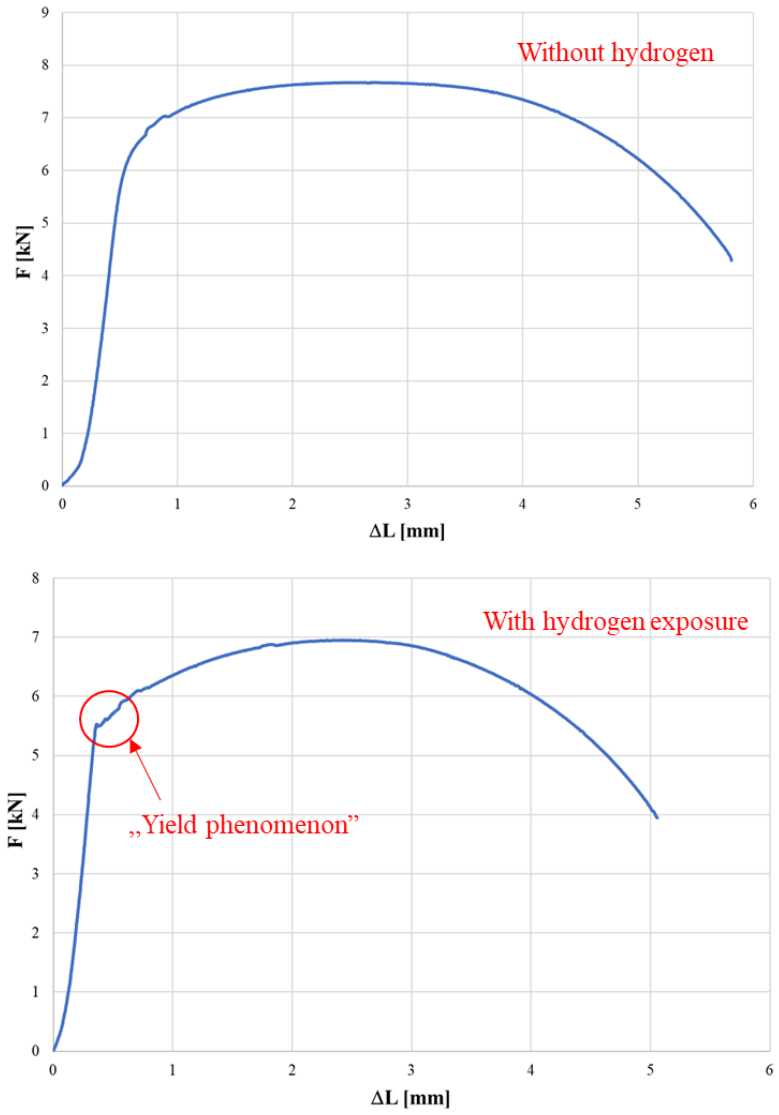

Figure 16. *Characteristic tensile diagrams of the base material without hydrogen and after exposure to hydrogen*

6. Summary

The effect of hydrogen on steel and welded joints of P355NH can be concluded as follows.

1. Changes can be observed in the microstructure of both the base material and the welded joints under the influence of hydrogen.
2. Based on the results of hardness measurements, it can be said that for 41 and 92 days of exposure to hydrogen, the duration of exposure has no significant effect on either the material or the welded joints.
3. For the base material, a greater increase in hardness was observed in perlite than in ferrite.

4. In the case of GMAW joints, higher hardness values were typically measured in the heat-affected zones after exposure to hydrogen. For GMAW joints, the grain growth and recrystallized zones are the critical microstructural regions, for GTAW joints the grain growth zone is critical for the steel tested.
5. Based on the hardness tests, the joints of the P355NH steel tested with the GTAW technology are less sensitive and therefore the risk of hydrogen-induced embrittlement is expected to be lower for this type of joint.
6. The results of the tensile tests show that the duration of exposure to hydrogen at exposure times of 41 and 92 days has no significant effect on the tensile test results, but for the P355NH steel tested, the decrease in strain parameters and increase in strength parameters clearly point towards embrittlement.

References

[1] Anijdan, S. M., Arab, G., Sabzi, M., Sadeghi, M., Eivani, A., & Jafarian, H. (2021). Sensitivity to hydrogen induced cracking, and corrosion performance of an API X65 pipeline steel in H2S containing environment: influence of heat treatment and its subsequent microstructural changes. *Journal of Materials Research and Technology/Journal of Materials Research and Technology*, *15*, 1–16. **https://doi.org/10.1016/j.jmrt.2021.07.118**

[2] Beachem, C. D. (1972). A new model for hydrogen-assisted cracking (hydrogen "embrittlement"). *Metallurgical and Materials Transactions B*, *3*(2), 441–455. **https://doi.org/10.1007/BF02642048**

[3] Brass, A.-M., Chene, J., & Coudreuse, L. (2000). Fragilisation des aciers par l'hydrogène : mécanismes. *Corrosion Vieillissement*. **https://doi.org/10.51257/a-v2-m176**

[4] Cabrini, M., Coppola, L., Lorenzi, S., Testa, C., Carugo, F., Bucella, D. P., & Pastore, T. (2020). Hydrogen Permeation in X65 Steel under Cyclic Loading. *Materials*, *13*(10), 2309. **https://doi.org/10.3390/ma13102309**

[5] Chan, S. L. I., Lee, H. L., & Yang, J. R. (1991). Effect of retained austenite on the hydrogen content and effective diffusivity of martensitic structure. *Metallurgical Transactions A*, *22*(11), 2579–2586. **https://doi.org/10.1007/BF02851351**

[6] Choo, W. Y., & Jai Young Lee. (1983). Effect of cold working on the hydrogen trapping phenomena in pure iron. *Metallurgical Transactions. A, Physical Metallurgy and Materials Science*, *14*(7), 1299–1305. **https://doi.org/10.1007/BF02664812**

[7] Cotterill, P. (1961). The hydrogen embrittlement of metals. *Progress in Materials Science*, *9*(4), 205–301. **https://doi.org/10.1016/0079-6425(61)90005-6**

[8] Fallahmohammadi, E., Bolzoni, F., Fumagalli, G., Re, G., Benassi, G., & Lazzari, L. (2014). Hydrogen diffusion into three metallurgical microstructures of a C–Mn X65 and low alloy F22 sour service steel pipelines. *International Journal of Hydrogen Energy*, *39*(25), 13300–13313. **https://doi.org/10.1016/j.ijhydene.2014.06.122**

[9] Fukai, Y., Y. Shizuku, & Kurokawa, Y. (2001). Superabundant vacancy formation in Ni–H alloys. *Journal of Alloys and Compounds*, *329*(1-2), 195–201. **https://doi.org/10.1016/s0925-8388(01)01603-6**

[10] Hydrogen in Metals III. (1997). In *Springer eBooks*. Springer Nature. **https://doi.org/10.1007/BFb0103398**

[11] Ichimura, M., Yasushi Sasajima, & Mamoru Imabayashi. (1991). Grain boundary effect on diffusion of hydrogen in pure aluminum. *Materials Transactions, JIM*, *32*(12), 1109–1114. **https://doi.org/10.2320/matertrans1989.32.1109**

[12] Newman, J. F., & Shrier, L. L. (2010). Effect of carbon content and structure in CF steel on solubility and diffusion coefficient of hydrogen. *J Iron Steel Inst*, *207*, 1369–1372.

[13] Jiang, Y., Li, C., Wang, D., & Di, X. (2021). Effect of cyclic plastic deformation on hydrogen diffusion behavior and embrittlement susceptibility of reeling-pipeline steel weldments. *International Journal of Hydrogen Energy*, *46*(58), 30158–30172. **https://doi.org/10.1016/j.ijhydene.2021.06.135**

[14] Lukács, J., & Dakhel, A. Y. (2024). Full-scale Fatigue and Burst Tests on Notched Pipeline Girth Welds, under Complex Loading Conditions. *Acta Polytechnica Hungarica*, 21(5), 53–70. **https://doi.org/10.12700/APH.21.5.2024.5.5**

[15] Luu, W. C., & Wu, J. K. (1996). The influence of microstructure on hydrogen transport in carbon steels. *Corrosion Science*, *38*(2), 239–245. **https://doi.org/10.1016/0010-938X(96)00109-6**

[16] Lynch, S. P. (1988). Environmentally assisted cracking: Overview of evidence for an adsorption-induced localised-slip process. *Acta Metallurgica*, *36*(10), 2639–2661. **https://doi.org/10.1016/0001-6160(88)90113-7**

[17] Parvathavarthini, N., Saroja, S., & Dayal, R. K. (1999). Influence of microstructure on the hydrogen permeability of 9%Cr–1%Mo ferritic steel. *Journal of Nuclear Materials*, *264*(1-2), 35–47. **https://doi.org/10.1016/S0022-3115(98)00486-3**

[18] Olden, V., Alvaro, A., & Akselsen, O. M. (2012). Hydrogen diffusion and hydrogen influenced critical stress intensity in an API X70 pipeline steel welded joint – Experiments and FE simulations. *International Journal of Hydrogen Energy*, *37*(15), 11474–11486. **https://doi.org/10.1016/j.ijhydene.2012.05.005**

[19] Oriani, R. (1970). The diffusion and trapping of hydrogen in steel. *Acta Metallurgica*, *18*(1), 147–157. **https://doi.org/10.1016/0001-6160(70)90078-7**

[20] Park, G. T., Koh, S. U., Jung, H. G., & Kim, K. Y. (2008). Effect of microstructure on the hydrogen trapping efficiency and hydrogen induced cracking of linepipe steel. *Corrosion Science*, *50*(7), **1865–1871. https://doi.org/10.1016/j.corsci.2008.03.007**

[21] Proceedings of the First International Conference on Current Solutions to Hydrogen Problems in Steels, Washington DC, November 1-5, 1982

[22] Pundt, A., & Kirchheim, R. (2006). Hydrogen in metals: Microstructural Aspects. *Annual Review of Materials Research*, *36*(1), 555–608.

https://doi.org/10.1146/annurev.matsci.36.090804.094451

[23] Sakamoto, Y., & Mantani, T. (1976). Effect of quenching and tempering on diffusion of hydrogen in carbon steel. *Transactions of the Japan Institute of Metals*, *17*(11), 743–748. **https://doi.org/10.2320/matertrans1960.17.743**

[24] Stalheim, D. G., & Hoh, B.: *Guidelines for production of API pipelines steels suitable for hydrogen induced cracking (HIC) service applications*, 2010 8th International Pipeline Conference, Volume 2. **https://doi.org/10.1115/IPC2010-31299**

[25] Takai, K., Shoda, H., Suzuki, H., & Nagumo, M. (2008). Lattice defects dominating hydrogen-related failure of metals. *Acta Materialia*, *56*(18), 5158–5167. **https://doi.org/10.1016/j.actamat.2008.06.031**

[26] Tau, L., & Chan, S. L. I. (1996). Effects of ferrite/pearlite alignment on the hydrogen permeation in a AISI 4130 steel. *Materials Letters*, 29(1-3), 143–147. **https://doi.org/10.1016/s0167-577X(96)00140-1**

[27] Westlake, D G. *Generalized model for hydrogen embrittlement*. United States.